energies

MDPI

Article

CFD Modeling as an IT-Support Tool for NO_x Emission Reduction at Coal-Fired Thermal Power Plants

Symbat Bolegenova [1], Aliya Askarova [1], Saltanat Bolegenova [1], Aizhan Nugymanova [1,*], Valeriy Maximov [1], Nariman Askarov [1,2] and Shynar Ospanova [1]

[1] Department of Thermal Physics and Technical Physics, Farabi University, Al-Farabi Av., 71, Almaty 050040, Kazakhstan; bolegenova.symbat@kaznu.edu.kz (S.B.); aliya.askarova@kaznu.edu.kz (A.A.); saltanat.bolegenova@kaznu.edu.kz (S.B.); valeriy.maximov@kaznu.edu.kz (V.M.); aijoka01@gmail.com (N.A.); shynarospanova1987@gmail.com (S.O.)

[2] Kazatomprom National Atomic Company, 17/12, Syganak Street, Astana Z05T1X3, Kazakhstan

* Correspondence: nugymanova.aizhana@gmail.com; Tel.: +7-707-899-98-41

Abstract

In recent years, a sharp increase in coal-based power generation has been observed in a number of countries. Coal-fired thermal power plants remain the main source of harmful emissions in the energy sector of many countries, including Kazakhstan. This creates a strong need for the development of effective methods to reduce pollutant emissions at thermal power plants. The aim of the present study is to perform a numerical investigation of the effectiveness of staged combustion technology with secondary air injection (Over-Fire Air, OFA) applied to three boilers—PK-39, BKZ-160, and BKZ-75—which differ in design, capacity, and furnace configuration. CFD modeling was carried out using the FLOREAN package, adapted to the conditions of the Kazakh energy sector, which relies on high-ash coal (more than 40%) for coal-based power generation. Model validation was performed against experimental data obtained from operating thermal power plants. It was found that air injection through OFA injectors intensifies turbulent mixing, reduces peak temperatures in the main combustion zone, and ensures a more uniform distribution of heat release along the furnace height, thereby suppressing thermal NOx formation. It is shown that the spatial structure of NO concentration fields at the furnace outlet strongly depends on the design features of each boiler. The results demonstrate the high efficiency of staged combustion technology in reducing nitrogen oxide emissions and improving the environmental performance of pulverized-coal boiler units. The obtained results can be used in the design of new and the modernization of existing thermal power plants utilizing coal-based power generation.

Keywords: coal-fired generation; harmful emissions; staged combustion

Check for updates

Academic Editors: Shujun Zhu, Shuai Guo, Zhuozhi Wang and Lianfei Xu

Received: 25 May 2026
Revised: 19 June 2026
Accepted: 25 June 2026
Published: 29 June 2026

Copyright: © 2026 by the authors. Licensee MDPI, Basel, Switzerland. This article is an open access article distributed under the terms and conditions of the Creative Commons Attribution (CC BY) license.

1. Introduction

Despite the world's leading countries announcing their plans for carbon neutrality by 2020–2060, coal production shows no signs of slowing down. This is primarily due to high natural gas prices, huge demand for electricity, and the accelerated development of energy and industry in China, India, and Southeast Asia [1].

The International Energy Agency's report for the first half of 2025 predicts that global coal consumption will remain at historically high levels in 2025 and 2026 (Figure 1). Global coal demand reached a new all-time high in 2024, reaching approximately 8.77 billion

tonnes, 1.5% higher than in 2023. Coal-fired electricity generation reached a record high of 10,766 TWh that same year [2].

Global Coal Consumption 2022–2026, Mt

Region/Country	2022	2023	2026	2021–22	2022–23	CAAGR 2023–2026
Asia Pacific	**6,639**	**6,971**	**6,967**	**5.3%**	**5.0%**	**0.0%**
China	4,520	4,740	4,535	4.6%	4.9%	-1.5%
India	1,162	1,260	1,397	9.1%	8.4%	3.5%
Japan	185	171	157	1.2%	-7.7%	-2.8%
ASEAN	413	444	528	13.2%	7.5%	6.0%
North America	**489**	**392**	**304**	**-6.9%**	**-19.7%**	**-8.1%**
United States	455	360	276	-7.6%	-20.9%	-8.4%
Central and South America	**48**	**38**	**35**	**-11.5%**	**-20.6%**	**-2.4%**
Europe	**671**	**561**	**456**	**4.3%**	**-16.5%**	**-6.7%**
European Union	461	354	278	3.9%	-23.3%	-7.7%
Eurasia	**368**	**378**	**379**	**1.0%**	**2.9%**	**0.1%**
Russia	249	258	250	4.5%	3.3%	-1.0%
Africa	**187**	**183**	**193**	**-2.3%**	**-2.2%**	**1.8%**
Middle East	**13**	**13**	**8**	**2.2%**	**-2.2%**	**-13.8%**
World	**8,415**	**8,536**	**8,344**	**4.0%**	**1.4%**	**-0.8%**

Notes:
CAAGR = Compound Average Annual Growth Rate.
Data for 2022 are preliminary; 2023 are estimated; 2024–2026 are forecasts.

Figure 1. World coal consumption in 2022–2026.

Global coal consumption in 2030 and 2050 will be higher than projected. The International Energy Agency has repeatedly revised its coal forecasts, as overall electricity consumption is growing faster than wind and solar generation. The growth in coal demand will primarily come from the rapidly growing economies of India and other developing countries in Asia and Africa. The world faces an inexhaustible need for electricity. The IEA warns that the growth of energy-intensive data centers, fueling the emergence of artificial intelligence, will likely further increase electricity demand in the coming years (Figure 2).

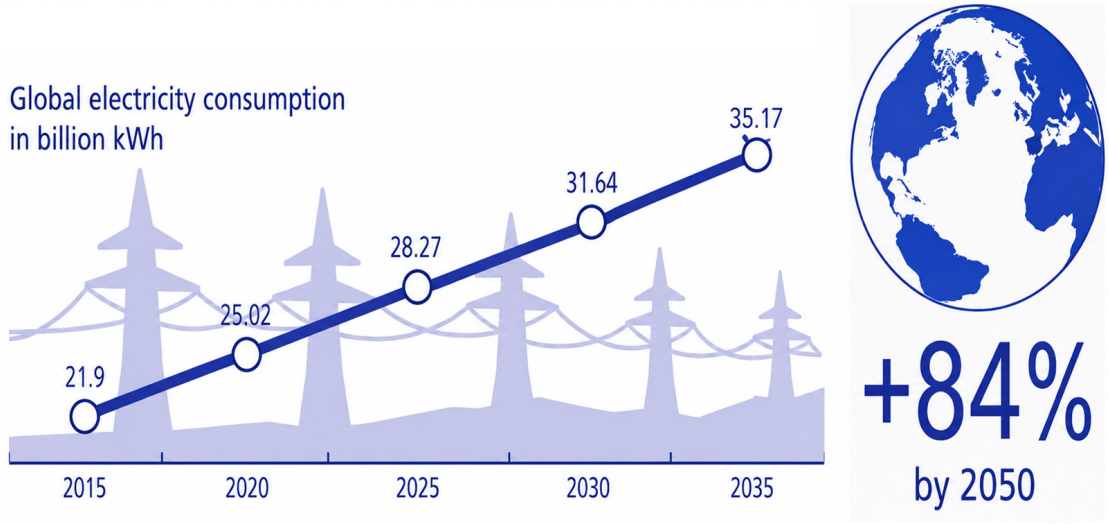

Figure 2. World electricity consumption in billions of kWh.

Many countries are suspending or cancelling their programs aimed at phasing out coal-fired power plants. At present, a rapid expansion of coal-based power generation is being observed in some countries. This growth indicates that energy security is temporarily

taking priority over climate-related discourse. The Middle East crisis has brought coal back to the forefront of the global energy mix. The top 10 countries by coal reserves are the United States, Russia, China, Australia, India, Germany, Ukraine, Kazakhstan, South Africa, and Indonesia.

As for Kazakhstan, it is also continuing to rely on coal-based power generation. In the coming years, Kazakhstan will not be able to abandon coal, as approximately 70% of its electricity generation is coal-based. The country's coal reserves are sufficient for about 300 years, and coal energy remains the backbone of the entire power system.

The Republic of Kazakhstan has approved a National Project Development of Coal-Based Power Generation, which includes the construction of 8 new coal-fired power plants with a total capacity of 5.3 GW, as well as the modernization and reconstruction of 11 existing power facilities with a total capacity of 2.5 GW [3,4].

According to experts, the bulk of decarbonization in Kazakhstan should occur between 2040 and 2060. In this regard, the National Project places particular emphasis on the use of "clean coal" technologies. It envisages the construction of highly efficient coal-fired power plants and the modernization of existing thermal power plants using advanced technological solutions and the introduction of modern coal combustion methods that will reduce pollutant levels [5].

Reducing NO_x emissions from high-ash coal combustion at Kazakhstan thermal power plants is a pressing scientific and practical challenge. Significant experience has been accumulated in CFD modeling of afterburning staged combustion (OFA) technology for various types of industrial and power boilers. The influence of OFA parameters on the flow structure and NO_x emissions has been studied for boilers with counter- and tangential burner arrangements [6–8], the design of burner devices has been optimized in conjunction with staged air supply [7], and the influence of deep staged combustion on the distribution of heat flows and NO_x in high-capacity boilers has been analyzed [8].

High ash content in coal significantly alters the kinetics of coke residue burnout and requires special adaptation of standard CFD combustion models, which is especially important for Kazakhstan coals with an ash content of >40%. Such an adaptation was previously performed by the authors of this work for the basic combustion mode [9], but its verification under staged combustion conditions with OFA has not been carried out. At the same time, the overwhelming majority of published works were performed for boilers of the same design type and for coals with a relatively low ash content (usually no more than 8–15%).

A comparative CFD analysis of the efficiency of the OFA technology for several structurally different industrial boilers operating on coal of the same high ash class (>40%), typical for the Kazakh power industry, has not been carried out previously. It is this gap that determines the purpose and scientific novelty of the present work: a quantitative comparison of the efficiency of staged combustion for the PK-39, BKZ-160 and BKZ-75 boilers when adapting the FLOREAN CFD model to the conditions of high-ash coal.

To address the stated problem, the present study employs CFD modeling based on the FLOREAN package (Braunschweig, Germany), a specialized tool for simulating reacting multiphase flows in geometrically complex domains, which has been widely validated for industrial pulverized-coal boilers [10–12]. The software solves a coupled system of conservation equations for mass, momentum, energy, and species using the finite volume method, with closure provided by the k–ε turbulence model and the eddy dissipation model (EDM) for combustion.

In contrast to expensive experimental studies on physical models, this approach makes it possible to reproduce the aerodynamics, heat transfer, and NO_x formation directly in the actual furnace geometry under varying OFA operating conditions. A necessary condition

for the reliability of the results is the adaptation of the model to the specific features of high-ash Kazakh coal, validation against full-scale measurements at operating thermal power plants, and a grid independence study—all three stages are implemented in the present work.

In this study, CFD modeling is applied to investigate the effectiveness of OFA technology for boilers PK-39, BKZ-160, and BKZ-75 operating on high-ash Kazakh coal (>40%). The selected boilers differ in design, capacity, and burner arrangement, which allows the influence of geometric and aerodynamic factors on the efficiency of staged combustion to be assessed.

The OFA operating principle is based on dividing the total air flow into two streams: the primary air is supplied at the level of the burner devices and forms a fuel-rich zone with a stoichiometric excess air coefficient ($\alpha < 1$), while additional above-flame air is introduced through specialized OFA injectors in the upper part of the furnace, ensuring the afterburning of incomplete combustion products. This process organization forms two functionally distinct zones: a reduction zone with a reduced O_2 concentration and reduced peak temperatures, in which NO_x formation is suppressed, and an afterburning zone with excess air, where complete oxidation of the fuel is completed [7].

The reduction in NO_x emissions using OFA technology (Figure 3) is achieved through three interrelated mechanisms. First, a decrease in the maximum flame temperature limits the thermal formation of NO via the Zeldovich mechanism, the rate of which is exponentially dependent on temperature. Second, the reducing atmosphere of the primary zone initiates reactions of reduction of the formed NO to molecular nitrogen N_2 upon interaction with hydrocarbon radicals CH_3. Third, the delay in contact of fuel nitrogen with molecular oxygen reduces the conversion of nitrogen-containing compounds of the organic matter of coal to NO_x [13–20].

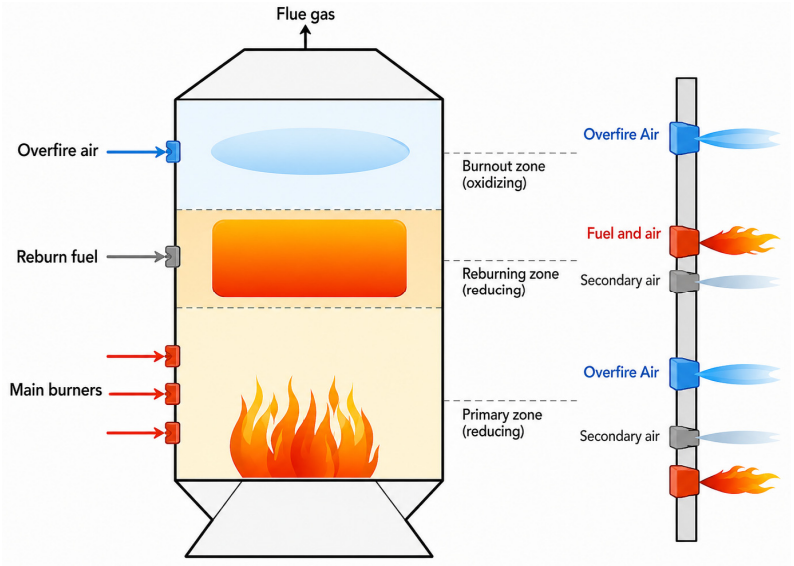

Figure 3. OFA injector arrangement configurations.

At an optimal fraction of secondary air supply in the range of 15–30% of the total air flow, and with a rational arrangement of the injectors, the combined effect of these mechanisms results in a 30–50% reduction in NO_x emissions compared to conventional combustion, without a significant increase in unburned carbon in the fly ash.

At the same time, the quantitative performance of the technology strongly depends on the design features of the specific boiler unit, including furnace geometry, burner arrangement, the elevation of OFA injectors, and their aerodynamic characteristics. This necessitates case-specific numerical investigations for each considered installation.

Unlike most published studies on OFA technology in single-type boilers, the present work is the first to perform a comparative CFD analysis for three structurally different boiler units—PK-39, BKZ-160, and BKZ-75-operating on high-ash Kazakh coal (ash content > 40%), for which standard CFD settings require specific adaptation. This makes it possible to identify the influence of boiler design features on OFA performance and to propose generalized recommendations for Kazakh coal-based power generation.

The study investigates the effect of secondary air injection through OFA injectors on the aerodynamic flow structure, temperature fields, and the distribution of nitrogen oxide (NO) concentrations along the furnace height and at the outlet section of the combustion chamber. The objectives of the study include: (1) adaptation of the FLOREAN CFD model to high-ash combustion conditions; (2) validation of the model against experimental data from operating thermal power plants; and (3) quantitative assessment of NO_x reduction under different OFA injector configurations for each boiler.

The obtained results make it possible to optimize the combustion processes of high-ash energy coal, reduce dust and gas emissions into the atmosphere, and facilitate the implementation of clean energy technologies at any energy facilities both in Kazakhstan and in other countries with coal-fired energy generation.

2. Materials and Methods

2.1. Mathematical Model

Numerical modeling of combustion processes in the furnaces of pulverized-coal boilers is based on a system of conservation equations for mass, momentum, energy, and gaseous species concentrations. A detailed description of the underlying mathematical model, including the formulation of boundary conditions and validation of the computational approach, is presented in the authors' previous work [9].

In the present section, only the key aspects of the model required for understanding the results are provided, together with a detailed description of the components that were extended or modified for the simulation of staged combustion with secondary air injection.

In a generalized conservative form, the system of equations for describing combustion processes in combustion chambers is written as follows [21–27]:

$$\frac{\partial \rho \varphi}{\partial t} = -\frac{\partial \rho u_i \varphi}{\partial x_i} + \frac{\partial}{\partial x_i}\left(\Gamma_\varphi \frac{\partial \varphi}{\partial x_i}\right) + S_\varphi, \quad (1)$$

where φ—transport variable (u, v, w, T, C, k, ε); Γ_φ—transfer coefficient; S_φ—a source term that takes into account chemical reactions, radiant heat transfer, and interphase interactions. The numerical solution is implemented using the finite volume method [21–31]. To close the system, the standard k–ε turbulence model with standard constants is used: $C_1 = 1.44$; $C_2 = 1.92$; $C_\mu = 0.09$; $\sigma_k = 1.0$; $\sigma_\varepsilon = 1.3$ [21,22,32]. The turbulence intensity at the inlet boundaries is taken to be Tu = 5%, which corresponds to typical conditions at the inlet of industrial boiler burners [21,22,33]. To simulate radiative heat transfer, which plays a dominant role in the combustion chambers of industrial boilers, a six-flow model of the flow method proposed by Lockwood [34] is used. This model approximates the distribution of radiant energy flux using power series and spherical functions, providing acceptable accuracy at moderate computational costs.

The pressure-velocity coupling is handled using the SIMPLE algorithm. The calculations are performed under steady-state conditions; convergence is defined by the reduction of normalized residuals for all governing equations below 10^{-4} [21,22].

The solved equations include conservation of mass (continuity), momentum in three spatial directions, energy (enthalpy), transport of gaseous species (O_2, CO_2, H_2O, CO,

volatiles), as well as the transport equations for turbulent kinetic energy (k) and its dissipation rate (ε).

2.2. Combustion Model of Pulverized Coal Fuel

In this work, the combustion process is described as a sequence of stages: pyrolysis with the release of volatile matter and the formation of a char residue; combustion of volatile products and carbon monoxide; and burnout of the char residue.

Pyrolysis is described using a single-step model [35], in which the volatile matter is represented as fictitious hydrocarbons with an empirical molecular formula. The combustion rate of the volatiles is determined within the framework of the Eddy Dissipation Model (EDM), proposed by Magnussen [36], which provides a robust description of turbulent combustion at moderate computational cost [37].

The adaptation of the FLOREAN package to the conditions of high-ash Kazakh coal (ash content > 40%) included the following modifications: (1) adjustment of volatile matter yield based on proximate and ultimate analysis of the coals used; (2) refinement of the char burnout rate to account for the increased content of mineral inclusions; and (3) adjustment of boundary conditions for the mass flow rate and temperature of the primary air in accordance with the operating maps of real thermal power plants. A detailed justification of the selected models and their validation for high-ash Kazakh coals is provided in [9].

In this study, particular attention is paid to the accurate representation of the interaction between secondary air jets and combustion products in the over-fire region. Under staged combustion conditions, the source term S_φ in Equation (1) is modified to account for the local variation in the excess air ratio along the furnace height, which is crucial for correctly predicting zones of reducing atmosphere formed below the level of the OFA injectors.

2.3. Model NOx

During the combustion of pulverized coal, nitrogen oxides are formed in various ways. The main contributors are the oxidation reactions of molecular nitrogen in the air (thermal NO_x formation) and fuel nitrogen (fuel NO_x). Figure 4 shows the accepted scheme for the conversion of nitrogen-containing compounds [10–12,21,37].

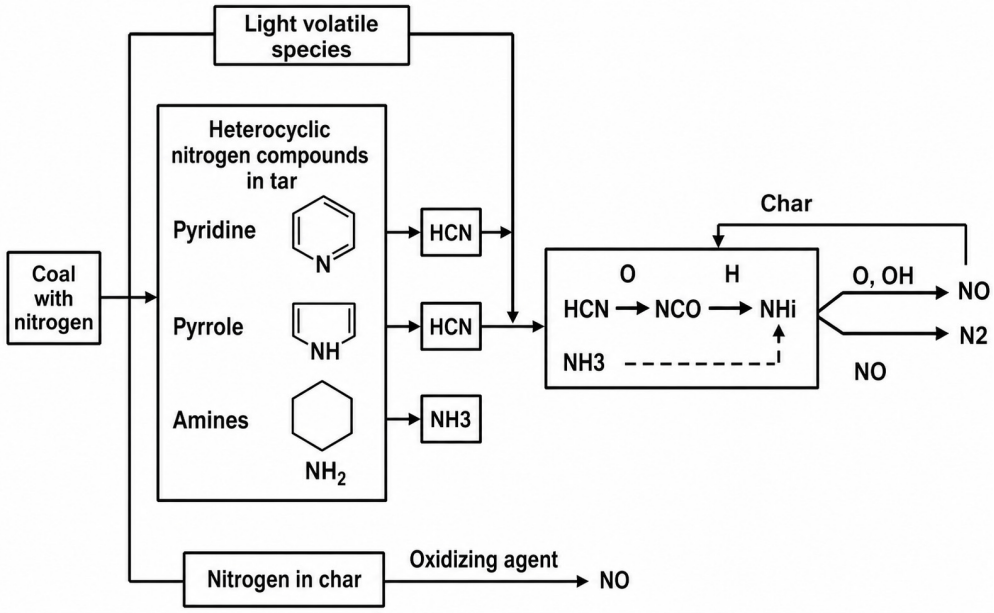

Figure 4. Scheme of transformation of nitrogen-containing compounds during coal combustion.

The mechanism of thermal NO_x formation is described according to the Zeldovich mechanism. The rate of thermal NO_x formation is calculated using a stable approximation for the concentration of N radicals, assuming that the concentration of O radicals is equal to the equilibrium concentration corresponding to the molecular dissociation of oxygen.

The main reaction responsible for fuel NO_x formation is the oxidation of fuel-bound nitrogen incorporated in complex organic compounds. It is assumed that these nitrogen-containing species are released during the devolatilization process. They are rapidly converted into hydrogen cyanide (HCN) or ammonia (NH_3). Nitrogen in the form of HCN or NH_3 may be released either through the reduction of NO to N_2 or through oxidation to NO.

Decomposition also occurs during the reburning of NO with hydrocarbons, leading again to the formation of HCN. Some authors have developed simplified models for calculating fuel NO concentrations in the combustible gas. De Soete proposed two reaction schemes involving two competing reactions for NO formation and destruction [38].

Mitchell and Tarbell [39] proposed a global mechanism for nitrogen-mediated reactions involving NH3, HCN, NO, and N_2 as nitrogen-containing components. The first step in the reaction is the conversion of HCN to NH_3 upon reaction with an oxidizer. The Mitchell and Tarbell model takes into account the recirculation of NO back to HCN upon interaction with hydrocarbons.

The NO_x concentration is calculated postprocessorically based on frozen temperature and gas mixture composition fields obtained from the main combustion calculation using the EDM. This approach is justified by the low NO concentration (on the order of ppm), which does not adversely affect the heat balance. Prompt NO via the Fennimore mechanism is accounted for through the reaction $CH + N_2 \rightarrow HCN + N$ in the flame front zone; its contribution under high-temperature pulverized coal combustion conditions is relatively small compared to the thermal and fuel mechanisms but is included for completeness. The connection between the NO_x model and combustion calculations is realized through the fields of local temperature T, concentrations of O_2, N_2, OH and CO calculated by the EDM.

2.4. Boundary Conditions for Secondary Air Supply Zones

Unlike the standard combustion problem formulation, modeling modes with OFA requires the specification of special boundary conditions at the inlet cross-sections of the OFA injectors. The secondary air velocity at the injector inlet is determined by maintaining the flow rate, considering the specified OFA fraction as a percentage of the total air flow rate required for fuel combustion:

$$u_{OFA} = \frac{\dot{m}_{OFA}}{\rho_{air} A_{OFA}}, \quad (2)$$

where $\dot{m}_{OFA}$—secondary air mass flow rate; A_{OFA}—the total cross-sectional area of the injectors. The secondary air temperature was assumed to be equal to the air temperature after the air heater. The kinetic energy of turbulence and its dissipation rate at the injector inlet were specified similarly to the conditions on the main burner devices with a degree of turbulence T_u = 5%.

At the outlet boundaries of the furnace chamber, free outflow conditions are applied: the gradients of all variables in the direction normal to the boundary are set to zero. In symmetry planes, the normal velocity components and the normal gradients of all variables are set to zero. No-slip boundary conditions are imposed on the solid furnace walls, together with standard wall functions for turbulent variables. Thermal boundary conditions are specified either as a fixed wall temperature (T_w), or as a prescribed heat flux (q_w).

Thus, the presented mathematical model provides a comprehensive description of the aerodynamic, thermal and chemical-kinetic processes in the combustion chamber, taking into account the specifics of staged combustion, which is a necessary condition for reliable prediction of NO_x emissions at different fractions of secondary blast.

2.5. Study of Combustion Processes in a Combustion Chamber Using Physical and CFD Modeling Methods

For the numerical study, the combustion chambers of the following boilers were considered: PK-39, BKZ-160, and BKZ-75, operated at thermal power plants in Kazakhstan. The selected boiler units are characterized by different combustion process organization schemes, including thermal power, burner device layout, fuel, oxidizer, and OFA injector delivery methods, as well as combustion chamber geometric dimensions (Figure 5).

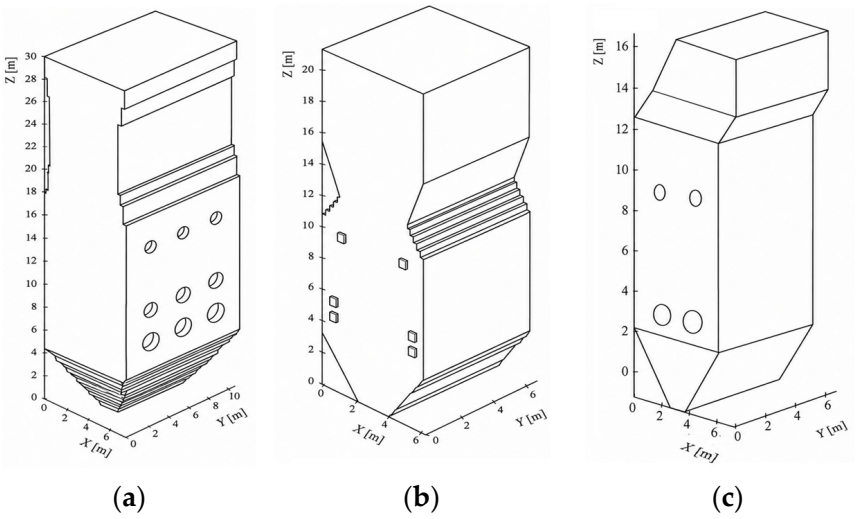

Figure 5. Scheme of combustion chambers of boilers: PK-39 (**a**), BKZ-160 (**b**) and BKZ-75 (**c**).

The study investigates the effectiveness of staged combustion technology with secondary air injection (Over-Fire Air, OFA) for reducing nitrogen oxide (NO_x) emissions. A comparative analysis is performed to assess the influence of OFA supply on the aerodynamic flow structure, temperature fields, and NO_x concentration distribution within the furnace volume. For each boiler, different secondary air injection regimes were considered, allowing the evaluation of how oxidizer redistribution affects combustion characteristics and the environmental performance of the boiler units.

Boundary conditions and input parameters for all simulation cases were defined based on operational data from existing thermal power plants. The initial data used in the numerical modeling of fuel combustion processes, as well as the main characteristics of the furnace chambers and coal particles, are presented in Table 1.

Figure 6 presents the finite-difference grids of the furnace chambers of the investigated boilers PK-39, BKZ-75, and BKZ-160, obtained by discretizing the computational domain into control volumes. The number of control volumes is determined by the furnace geometry, its dimensions, the arrangement of the burner systems, and the configuration of the secondary air (OFA) injection system.

After conducting preliminary numerical experiments to assess the influence of mesh resolution on the simulation results, optimal computational domain parameters were selected. The criterion for grid independence was defined as a change in NO concentration at the furnace outlet of less than 2% when refining the mesh to a finer resolution. For the PK-39 boiler at the Aksu TPP, the computational grid consisted of 98,820 control volumes with dimensions of 27 × 61 × 60.

Table 1. Technical characteristics of boilers and coal composition.

Nomination	**PK 39**			**BKZ 160**			**BKZ 75**
Height, m	29.985			21.000			16.75
Width, m	10.76			6.565			6
Depth, m	7.762			7.168			6.6
Number of boiler burners, pcs.	12			8			4
Number of tiers, pcs.	2			2			1
Air mixture temperature, °C	150			250			140
Fuel consumption for the boiler, t/h	87.5			30			12.49
Fuel consumption per burner, t/h	7.292			3.75			3.122
Boiler	Coal composition (mass fraction)						
	Water	Ash	C	H	O	N	S	Coal
PK 39	0.070	0.409	0.432	0.030	0.048	0.006	0.005	ekibastuz1
BKZ 160	0.058	0.397	0.441	0.031	0.061	0.007	0.005	ekibastuz2
BKZ 75	0.106	0.314	0.478	0.034	0.058	0.006	0.004	karaganda

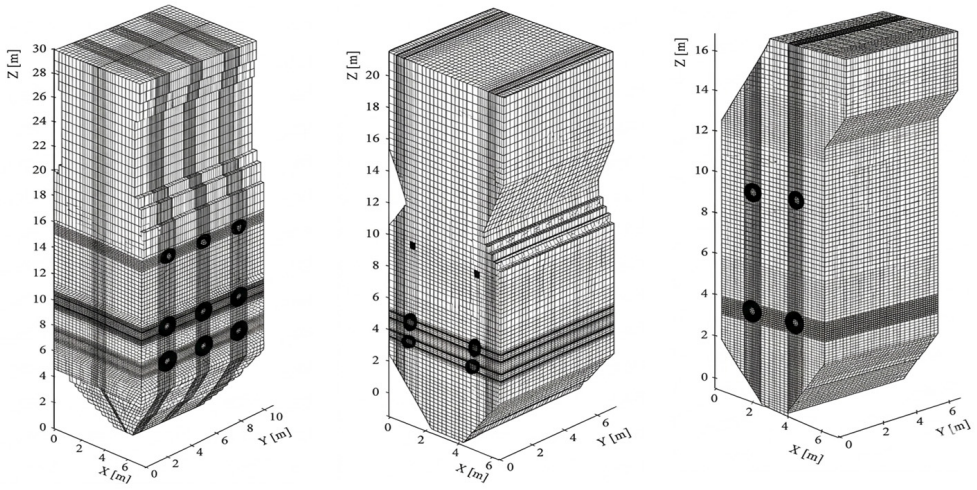

(**a**) (**b**) (**c**)

Figure 6. Breakdown of combustion chambers: PK-39 (**a**), BKZ-160 (**b**) and BKZ-75 (**c**) into control volumes for numerical modeling.

For the BKZ-160 boiler, a computational grid with parameters of 41 × 36 × 45 was used, providing 66,420 control volumes. For the BKZ-75 boiler, a finite-difference grid of dimensions 90 × 32 × 158 was used, corresponding to 455,040 control volumes. Mesh refinement was applied in the regions of fuel and air injection, as well as near the furnace walls. The structured meshes used are characteristic of the FLOREAN 5.0 package, where similar resolutions have been successfully applied in validated simulations of industrial pulverized-coal boilers [10–12]. The relatively lower number of control volumes for the BKZ-160 boiler is compensated by the smaller furnace size (21 m) and by validation against full-scale experimental data. This confirms the adequacy of the adopted resolution for predicting the mean flow characteristics and NO_x concentration distribution.

For the numerical simulation of heat and mass transfer processes in the furnace chambers of thermal power plant boilers, the FLOREAN software package (Germany) [10–12,21] was used. It is a specialized tool for simulating reacting multiphase flows in geometrically complex domains and is widely applied in the study of combustion processes in various types of thermal power engineering systems.

A methodology for adapting the FLOREAN package to the conditions of the Kazakh energy sector was developed. This adaptation was necessary due to significant differences between Kazakh and German coals: in particular, the ash content of domestic fuel can reach up to 50%, whereas for German coals this parameter typically does not exceed 8%.

Additional differences are related to the design features of furnace chambers, burner configurations, and fuel and air supply schemes typical of Kazakh power plants. Taking these factors into account, the original FLOREAN code was modified, functionally extended, and validated for high-ash coal combustion, ensuring the reliability of the obtained numerical results.

Using CFD modeling of the furnace chambers, an assessment of the effectiveness of staged combustion technology was carried out by varying the fraction of air supplied through over-fire air (OFA) injectors. The simulations were performed for three boilers under the following OFA values expressed as a percentage of the total air flow required for fuel combustion:

PK-39 (0%—baseline case, 10% and 20%);

BKZ-160 (0%—baseline case, 10% and 20%);

BKZ-75 (0%—baseline case, 5% and 18%).

The OFA variation ranges for each boiler were determined individually. For the BKZ-75 boiler, the upper limit was set at 18% instead of 20% for two reasons: the smaller furnace height (16.75 m) limits the length of the reducing zone and, at OFA fractions above 18%, leads to incomplete fuel burnout; additionally, the lower temperature level of the process (885 °C compared to 1114–1239 °C for the other boilers) means that even a small redistribution of air significantly affects the completeness of combustion.

Table 2 presents the calculated mass flow rates of secondary air through the OFA nozzles for each of the studied modes.

Table 2. Design characteristics of boilers with staged fuel combustion.

Characteristic	PK 39		BKZ 160		BKZ 75	
Number of OFA burners, pcs.	6		4		4	
Height of the lower burner tier, m	7.315		4.537		4	
Height of the upper burner tier, m	10.115		5.523			
Height of OFA burner tier, m	15.735		10		9.4	
OFA burner diameter, m	0.7		0.361		0.325	
Mass air flow through the OFA nozzle, kg/s	OFA—10% 4.5	OFA—20% 8.97	OFA—10% 4.007	OFA—20% 8.015	OFA—5% 0.186	OFA—18% 0.830

As a result of computational experiments, distributions of the total velocity vectors, temperature fields, and nitrogen oxide (NO) concentrations throughout the combustion chamber and at its outlet were obtained. Based on the obtained data, a comparative analysis of the modes under consideration was performed.

3. Results

Within the framework of the present study, a comprehensive analysis was performed of the influence of the air fraction supplied through OFA injectors on the thermal regime of the furnace chambers of the boiler units PK-39, BKZ-160, and BKZ-75, the completeness of fuel combustion, and the intensity of nitrogen oxide (NO) formation.

The simulations were carried out for each boiler at different values of secondary air supply: for PK-39 and BKZ-160—0%, 10%, and 20%; for BKZ-75—0%, 5%, and 18% of the total combustion air flow.

Based on the obtained results, it was established that variation in OFA injection parameters in all considered cases significantly affects the formation of temperature zones,

the mixing characteristics, the development of reducing conditions, and the efficiency of burnout processes.

A comparative analysis of the three boiler units showed that, despite differences in their design characteristics and in the ranges of variation in the secondary air flow, each of them has OFA injection regimes that provide a maximum reduction in NO concentration within the studied OFA fraction range (Table 3), while maintaining a stable furnace temperature regime. The effect of these operating conditions on the completeness of fuel burnout requires separate investigation and is considered a limitation of the present study.

Table 3. Average values of temperatures T and NO concentrations at the outlet of the furnaces.

Boiler		**PK-39**			**BKZ-160**			**BKZ-75**	
OFA, %	OFA—0	OFA—10	OFA—20	OFA—0	OFA—10	OFA—20	OFA—0	OFA—5	OFA—18
T, °C	1238.92	1220	1200	1113.7	1108.7	1106.7	885.80	868.10	856.27
NO, mg/Nm^3	527.78	477.01	423.29	498.38	427.68	351.69	368.08	364.30	277.12

The obtained data indicate that the two-stage combustion technology with controlled supply of additional air is an effective tool for reducing nitrogen oxide emissions and increasing the energy efficiency of boilers operating on high-ash Kazakh coal.

3.1. Computational Experiment to Study the Aerodynamics of the Flow in the Combustion Space of Three Boilers

Figure 7 shows the velocity vector distributions in the central longitudinal section of the furnace chamber of the PK-39 boiler for two operating regimes: without air supply through OFA injectors (Figure 7a, OFA = 0%, baseline case) and with air supply through OFA injectors (Figure 7b, OFA = 20%).

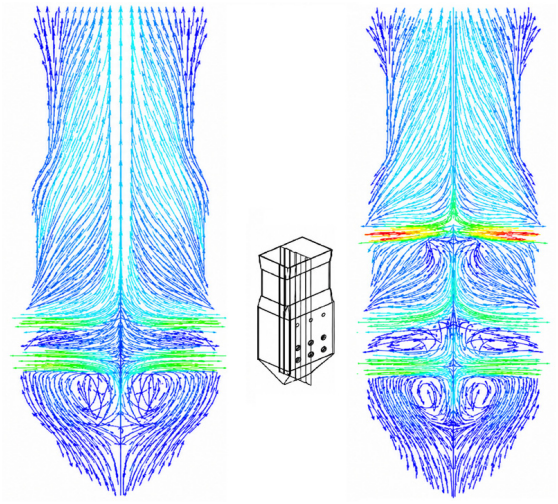

(**a**) (**b**)

Figure 7. The velocity vector field in the longitudinal section of the combustion chamber of the PK-39 boiler for different volumes of air supplied through the injectors: OFA = 0% (**a**) and OFA = 20% (**b**).

Analysis of Figure 7a,b shows that activation of the OFA injectors leads to a change in flame shape and a redistribution of velocity fields compared to the baseline regime. At OFA = 20% (Figure 7b), the main combustion zone shifts toward the central part of the furnace chamber, accompanied by a local increase in gas flow velocities. The high velocity of secondary air injection through the OFA injectors intensifies flow turbulence and leads to the formation of vortex structures in both near-wall and central regions, where interacting opposing jets are present.

A comparison of Figure 7a,b indicates that the use of OFA injectors significantly alters the aerodynamic structure of the flow: turbulent mixing is enhanced, the entrainment of peripheral flows into the central region increases, and the intensity of momentum exchange between furnace zones rises. This promotes a more uniform distribution of oxidizer, improves combustion conditions, and reduces the likelihood of incomplete combustion product formation.

Figure 8 shows the velocity vector distribution in the longitudinal section of the furnace chamber of the BKZ-160 boiler for the operating regimes OFA = 0% (Figure 8a) and OFA = 20% (Figure 8b).

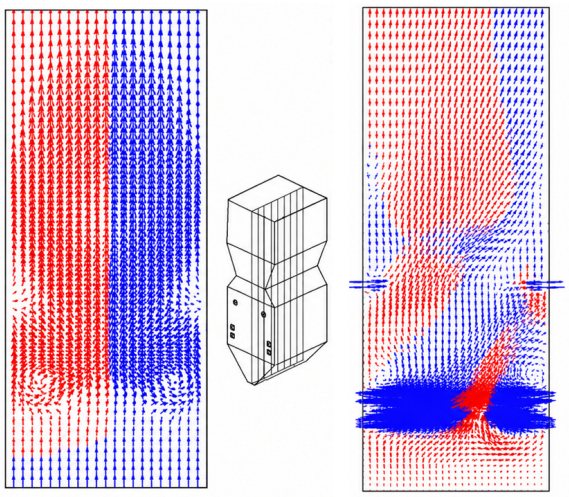

(**a**) (**b**)

Figure 8. The velocity vector field in the longitudinal section of the combustion chamber of the BKZ-160 boiler at different volumes of air supplied through the injectors: OFA = 0% (**a**) and OFA = 20% (**b**).

In the baseline regime (Figure 8a), a predominantly uniform upward axial flow of the gas-air mixture is observed, without pronounced regions of local turbulence. When the OFA injectors are activated (Figure 8b), intense horizontal jets are formed in the injection regions, penetrating into the central part of the furnace chamber and causing a redistribution of the velocity field.

The interaction of opposing jets leads to the formation of vortex structures that enhance turbulent mixing of the gas–air mixture. A comparison of Figure 8a,b shows that the use of OFA injectors intensifies aerodynamic processes within the furnace chamber. The increased turbulent mixing promotes more effective fuel-oxidizer interaction, improves combustion conditions, and reduces the likelihood of forming local oxygen-deficient zones.

Figure 9 illustrates the velocity vector distribution in the central section of the furnace chamber of the BKZ-75 boiler for the operating regimes OFA = 0% (Figure 9a) and OFA = 18% (Figure 9b).

In the baseline regime (Figure 9a), the flow develops predominantly along the vertical axis of the furnace, with the formation of symmetric recirculation zones in the lower part of the chamber. The intensity of transverse mixing remains limited.

When the OFA injectors are activated (Figure 9b), the flow structure becomes significantly more complex: additional jet streams are formed, and their interaction with the main upward flow leads to regions of increased turbulence and intensive vortex formation. The velocity field becomes less symmetric, and the penetration depth of the jets into the central region of the furnace increases.

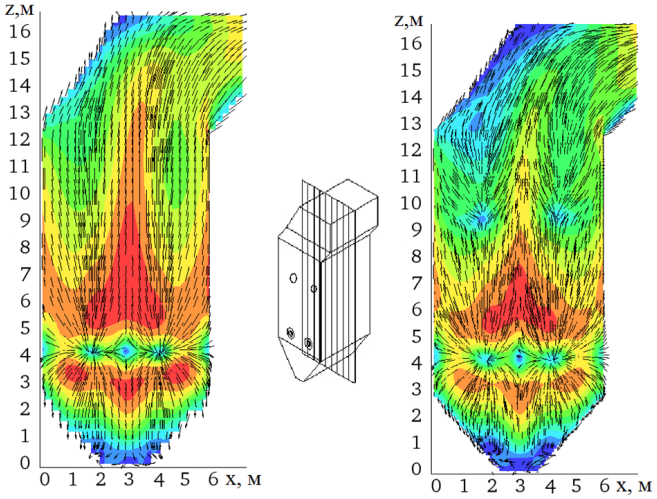

Figure 9. The velocity vector field in the longitudinal section of the combustion chamber of the BKZ-75 boiler at different volumes of air supplied through the injectors: OFA = 0% (**a**) and OFA = 18% (**b**).

A comparison of Figure 9a,b shows that the use of OFA injectors enhances turbulent mixing, improves oxygen distribution throughout the furnace volume, and reduces the likelihood of local oxidizer-deficient zones. This contributes to improved fuel burnout and reduced NO_x emissions.

A comparative analysis of the aerodynamic fields of the three boiler units reveals a fundamental dependence of flow restructuring on the furnace geometry.

In the PK-39 boiler with a large furnace height (30 m), the OFA jets mainly provide axial flow redistribution; their transverse penetration depth is limited, which reduces the effectiveness of forming a reducing zone across the entire cross-section.

In the BKZ-160 boiler with a compact geometry (21 m), the opposing jets reach the central region of the furnace, creating intensive transverse mixing and an extended zone with oxygen deficiency.

In the BKZ-75 boiler with a single-row burner arrangement, the flow restructuring is asymmetric, which directly leads to a bimodal NO profile along the furnace height.

Thus, the aerodynamic analysis establishes a causal relationship between chamber geometry, flow structure, and NO_x suppression efficiency. For boilers with tall furnaces, increasing the momentum and number of OFA jets is a priority, whereas for compact furnaces the key factor is the vertical positioning of the injectors.

3.2. Computational Experiment to Study Temperature Fields in the Combustion Space of Three Boilers

Figure 10 shows the temperature distribution in the central longitudinal section of the PK-39 boiler combustion chamber for the 0% OFA (Figure 10a) and 20% OFA (Figure 10b) modes. In the base mode (Figure 10a), a distinct high-temperature core with significant spatial heterogeneity and local temperature maxima forms in the zone of the main burners.

When the OFA injectors are activated (Figure 10b), a decrease in peak temperatures is observed in the lower part of the combustion chamber, the flame extends vertically, and the zone of maximum temperatures shifts upward along the chamber height. The stepped air supply ensures a more uniform heat distribution throughout the combustion chamber and promotes the formation of a stable flame structure.

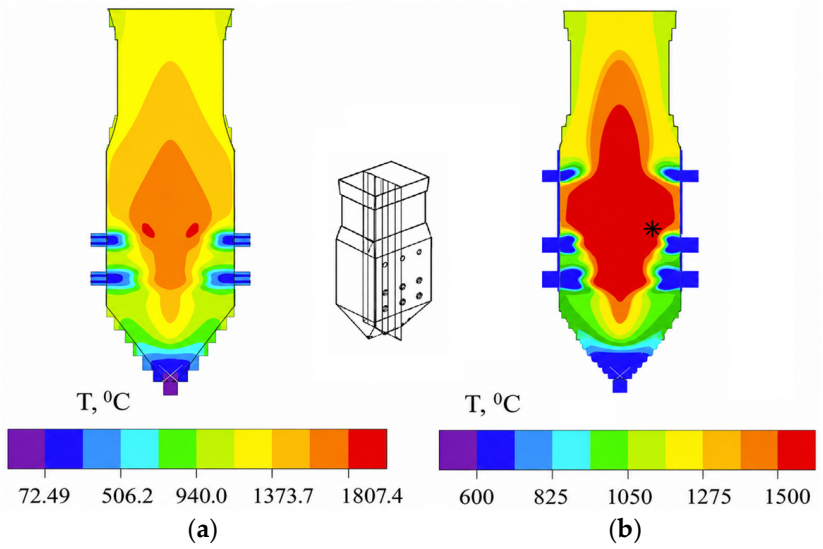

Figure 10. Temperature field in the longitudinal section of the combustion chamber of the PK-39 boiler at different volumes of air supplied through the injectors: OFA = 0% (**a**) and OFA = 20% (**b**). (*) indicate the monitoring points.

Figure 11 shows the temperature distribution in the longitudinal section of the BKZ-160 boiler combustion chamber for the 0% OFA (Figure 11a) and 20% OFA (Figure 11b) modes. In the base mode (Figure 10a), highly concentrated heat is generated in the burner zone with pronounced local temperature maxima.

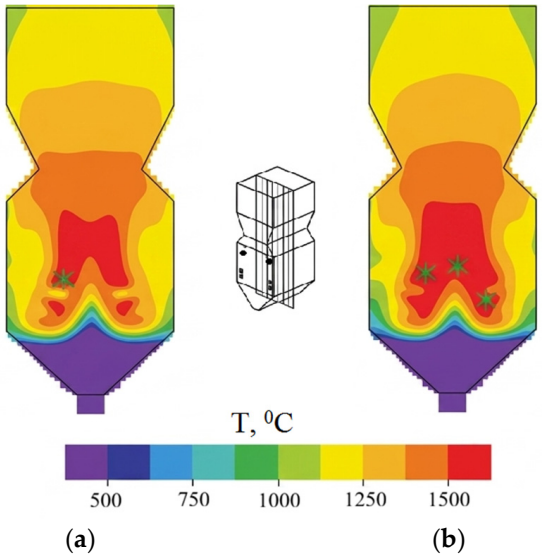

Figure 11. Temperature field in the longitudinal section of the combustion chamber of the BKZ-160 boiler at different volumes of air supplied through the injectors: OFA = 0% (**a**) and OFA = 20% (**b**). (*) indicate the monitoring points.

When the OFA injectors are activated (Figure 11b), a redistribution of the temperature profile is observed: the size of the high-temperature core decreases, and the zone of maximum temperatures shifts upward along the furnace height. A more uniform distribution of thermal stress throughout the chamber volume helps to reduce peak temperatures in the active combustion zone and the intensity of thermal NO_x formation.

Figure 12 shows the temperature field distribution in the longitudinal section of the BKZ-75 boiler combustion chamber for the 0% OFA (Figure 12a) and 18% OFA (Figure 12b) modes. In the base mode (Figure 12a), the combustion core is concentrated in the lower

part of the combustion chamber, with high thermal heterogeneity observed, contributing to localized overheating of the firebox screens and intensive formation of thermal NO_x.

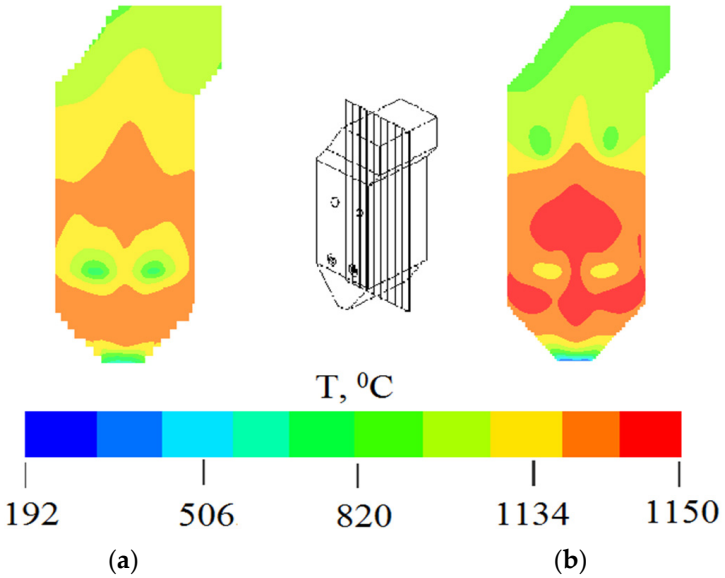

Figure 12. Temperature field in the longitudinal section of the combustion chamber of the BKZ-75 boiler at different volumes of air supplied through the injectors: OFA = 0% (**a**) and OFA = 18% (**b**).

When the OFA injectors are activated (Figure 12b), the temperature field structure changes significantly: the high-temperature zone expands and shifts upward along the furnace height, and the temperature gradients become more uniform. Intensification of afterburning processes in the supraburner zone contributes to increased fuel burnout and a reduction in mechanical underburning.

Figure 13 shows the change in temperature T along the combustion chamber height h for the following boiler units: PK-39 (Figure 13a), BKZ-160 (Figure 13b), and BKZ-75 (Figure 13c) at different values of the air fraction supplied through the OFA injectors, in comparison with the experimental data from full-scale tests.

A common pattern is observed for all three boilers: an increase in the OFA fraction leads to a decrease in peak temperatures at the bottom of the combustion chamber and a more uniform temperature distribution along the height. For the PK-39 boiler, maximum temperatures consistently decrease with an increase in the OFA fraction from 0% to 20%. A similar trend is observed for the BKZ-160 boiler, where activation of the injectors is accompanied by a smoothing of the temperature profile. For the BKZ-75 boiler, an increase in the OFA fraction to 18% ensures a leveling of the temperature field in the overburner zone.

The calculated curves are in satisfactory agreement with the experimental data [40,41], and for the BKZ-75 boiler with the theoretical value obtained by the CBTI method [42], which confirms the reliability of the applied CFD model. Thus, the use of OFA injectors for the PK-39, BKZ-160 and BKZ-75 boilers ensures a reduction in peak temperatures, equalization of the temperature profile along the height of the combustion chamber and a shift in the maximum temperature zone to the above-burner region, which helps suppress the thermal mechanism of NO_x formation and increase the efficiency of fuel combustion.

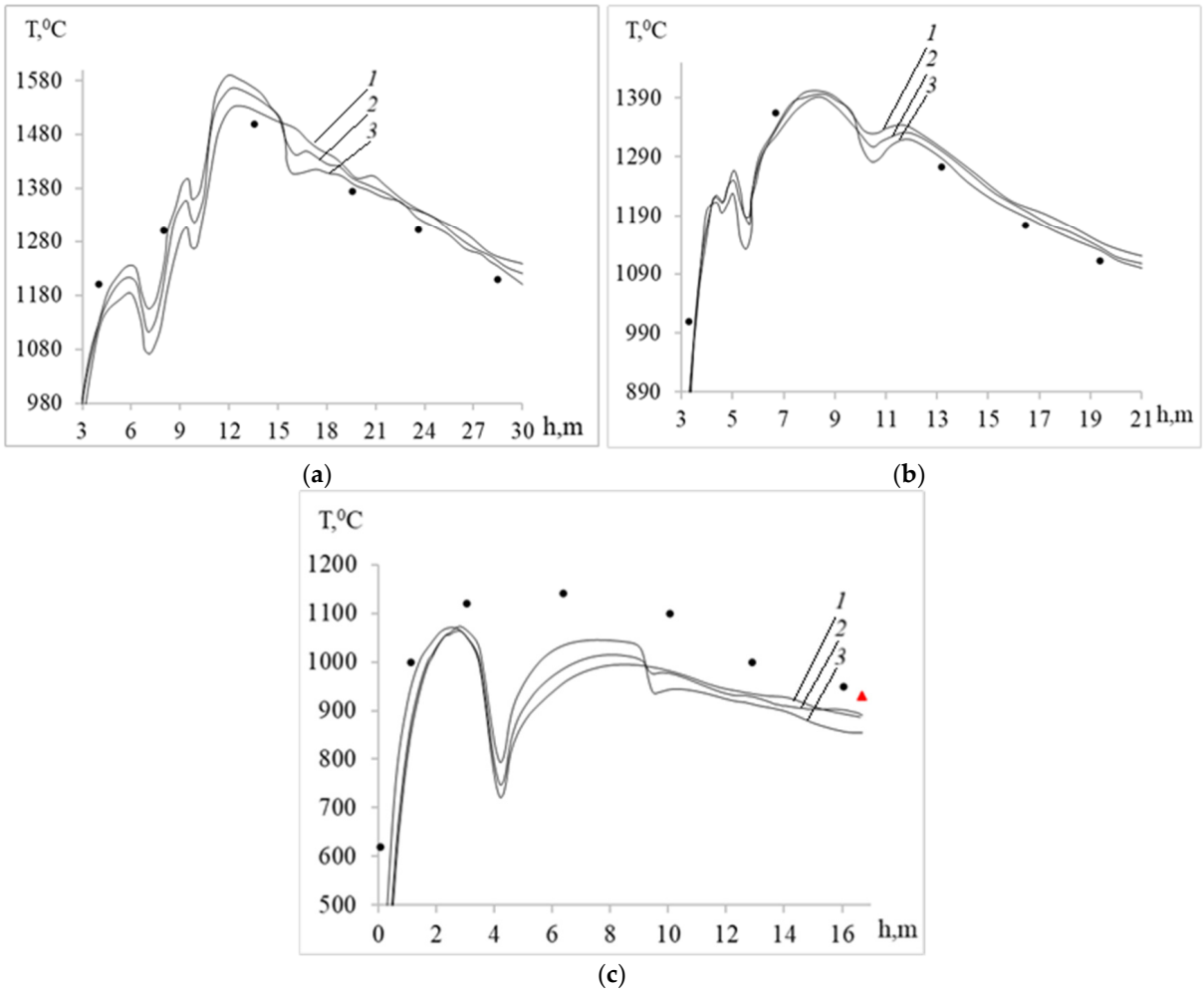

Figure 13. Temperature distribution T by the height of the combustion chamber of boilers: (**a**) PK-39: curve 1—OFA = 0%; curve 2—OFA = 10%; curve 3—OFA = 20%; ● —experiment at a thermal power plant [40]; (**b**) BKZ-160: curve 1—OFA = 0%; curve 2—OFA = 10%; curve 3—OFA = 20%; ● —experiment at a thermal power plant [41]; (**c**) BKZ-75: curve 1—OFA = 0%; curve 2—OFA = 18%; ● —experiment at a thermal power plant [41]; ▲ —theoretical value obtained by the CBTI method [42].

3.3. A Computational Experiment to Study the Processes of Nitrogen Oxide NO Formation in the Combustion Space of Three Boilers

Figures 14–16 show three-dimensional NO concentration fields in cross-section at the combustion chamber outlet of the PK-39, BKZ-160, and BKZ-75 boilers under different secondary air supply conditions. For all three boilers, a consistent decrease in maximum NO concentrations and a leveling of the distribution field are observed with an increase in the OFA share. However, the spatial structure of the zones of elevated concentrations is determined by the individual design features of each boiler unit.

Analysis of Figure 14 for the PK-39 boiler shows that in the baseline regime without air injection through the injectors (Figure 14a), the NO concentration field is characterized by pronounced non-uniformity. The average NO concentration at the furnace outlet is 527.78 mg/Nm^3 (Table 3).

With 10% air injection through the injectors (Figure 14b), the NO distribution becomes more uniform: regions of high concentration decrease, and the dominant range shifts to 375–450 mg/Nm^3. The average outlet NO concentration decreases to 477.01 mg/Nm^3, corresponding to a 9.6% reduction in emissions relative to the baseline regime.

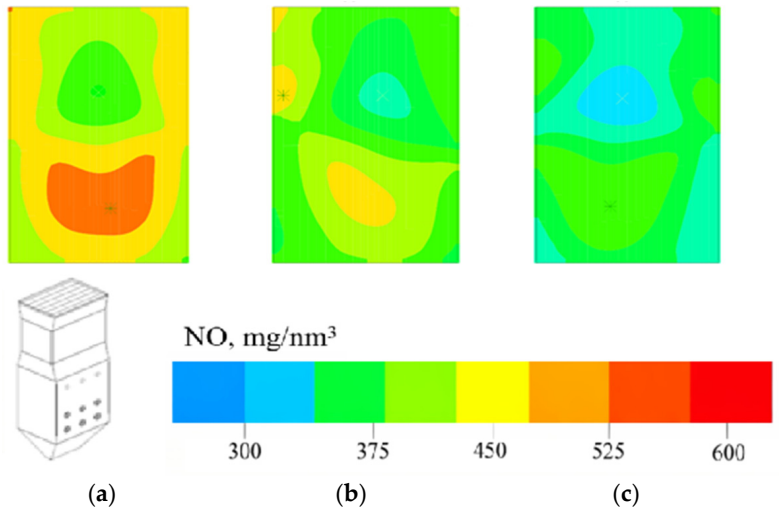

Figure 14. Distribution of nitrogen oxide concentration in the cross section at the outlet of the combustion chamber of the PK-39 boiler at different volumes of air supplied through the injectors: OFA = 0% (**a**), OFA = 10% (**b**) and OFA = 20% (**c**).

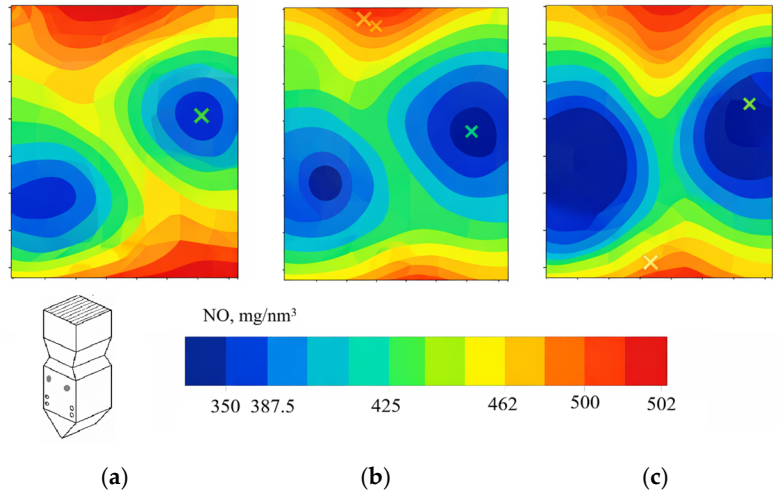

Figure 15. Distribution of nitrogen oxide concentration in the cross section at the outlet of the combustion chamber of the BKZ-160 boiler at different volumes of air supplied through the injectors: OFA = 0% (**a**), OFA = 10% (**b**) and OFA = 20% (**c**), ×—indicate the monitoring points used for NO concentration comparison.

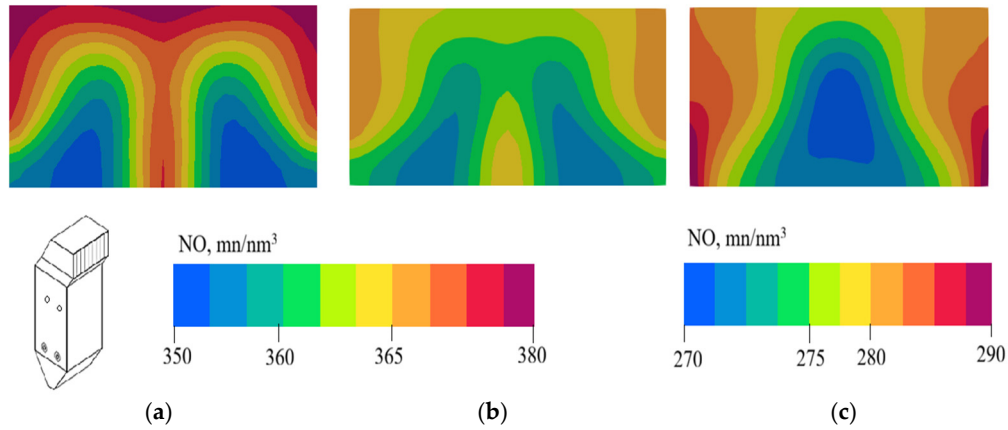

Figure 16. Distribution of nitrogen oxide concentration in the cross section at the outlet of the combustion chamber of the BKZ-75 boiler at different volumes of air supplied through the injectors: OFA = 0% (**a**), OFA = 5% (**b**) and OFA = 18% (**c**).

An increase in the over-fire air fraction to 20% (Figure 14c) leads to a further reduction in NO concentration and a more uniform field distribution. The dominant values lie in the range of 300–450 mg/Nm^3, while regions of elevated concentrations are practically absent. The average NO concentration at the furnace outlet decreases to 423.29 mg/Nm^3, which is 19.8% lower than the baseline case.

Thus, the application of OFA technology in the PK-39 boiler ensures a stable reduction in NO_x emissions with increasing secondary air fraction. An increase in OFA from 0% to 20% reduces the average outlet NO concentration from 527.78 to 423.29 mg/Nm^3 (19.8%), while simultaneously lowering the furnace temperature from 1238.92 °C to 1200 °C. This confirms the effectiveness of staged combustion in suppressing thermal NO_x formation.

Figure 15 presents the NO concentration distributions in the cross-section at the outlet of the furnace chamber of the BKZ-160 boiler under different over-fire air (OFA) injection regimes: Figure 15a—OFA = 0%; Figure 15b—OFA = 10%; and Figure 15c—OFA = 20%.

In the baseline regime (Figure 15a), the NO concentration field exhibits a symmetric structure with zones of reduced concentrations in the central part of the cross-section. Minimum values range from 350 to 387.5 mg/Nm^3, while in the peripheral and corner regions the concentration reaches 462–502 mg/Nm^3. The average NO concentration at the furnace outlet is 498.38 mg/Nm^3 (Table 3).

With 10% air injection through the injectors (Figure 15b), a redistribution of the concentration field is observed: regions of low concentration expand, while areas of high concentration decrease. The dominant range shifts to 387.5–462 mg/Nm^3. The average NO concentration at the outlet decreases to 427.69 mg/Nm^3, corresponding to a 14.2% reduction in emissions relative to the baseline case.

With an increase in the OFA fraction to 20% (Figure 15c), zones of reduced concentrations occupy a significant portion of the cross-section, especially in the corner regions. Despite a certain increase in the non-uniformity of the distribution compared to the OFA = 10% regime, the overall concentration level continues to decrease.

The average NO concentration at the outlet is 351.69 mg/Nm^3, which is 29.4% lower than the baseline case.

Thus, the OFA technology for the BKZ-160 boiler demonstrates high efficiency in reducing NO_x emissions. Increasing the over-fire air fraction from 0% to 20% reduces the average NO concentration at the furnace outlet from 498.38 to 351.69 mg/Nm^3 (29.4%), while the furnace temperature decreases only slightly—from 1113.7 °C to 1106.7 °C—indicating that the dominant mechanism of NO_x reduction under staged combustion is chemical rather than thermal suppression.

Figure 16 shows the NO concentration distributions in the cross-section at the outlet of the furnace chamber of the BKZ-75 boiler under different overfire air (OFA) injection conditions: Figure 16a—OFA = 0%; Figure 16b—OFA = 5%; and Figure 16c—OFA = 18%.

In the baseline operating mode (Figure 16a), the NO concentration is distributed unevenly, with zones of elevated values located in the burner region. The concentration range is 350–380 mg/Nm^3, and the average NO concentration at the furnace outlet is 368.08 mg/Nm^3 (Table 3).

When 5% of the air is supplied through the OFA injectors (Figure 16b), the overall distribution pattern remains similar; however, a slight decrease in NO concentration is observed. The average NO concentration at the furnace outlet decreases to 364.30 mg/Nm^3, corresponding to a reduction of approximately 1.0% compared to the baseline operating condition.

Increasing the OFA share to 18% (Figure 16c) results in a significant reduction in NO concentrations and a more uniform concentration field. The concentration range decreases

to 270–290 mg/Nm^3, while the average concentration reaches 277.12 mg/Nm^3, which is 24.7% lower than in the baseline operating mode.

Thus, the application of OFA technology in the BKZ-75 boiler provides effective NO_x emission reduction, similar to the results obtained for the previous two boilers. Increasing the share of overfire air from 0% to 18% reduces the average NO concentration at the furnace outlet from 368.08 to 277.12 mg/Nm^3 (24.7%), while simultaneously decreasing the furnace chamber temperature from 885.80 °C to 856.27 °C.

Figure 17 presents the results of two-dimensional modeling of the variation in NO concentration (mg/Nm^3) along the height of the furnace chamber for the RK-39 boiler (Figure 17a), the BKZ-160 boiler (Figure 17b), and the BKZ-75 boiler (Figure 17c) at different levels of air supply through the overfire air (OFA) nozzles.

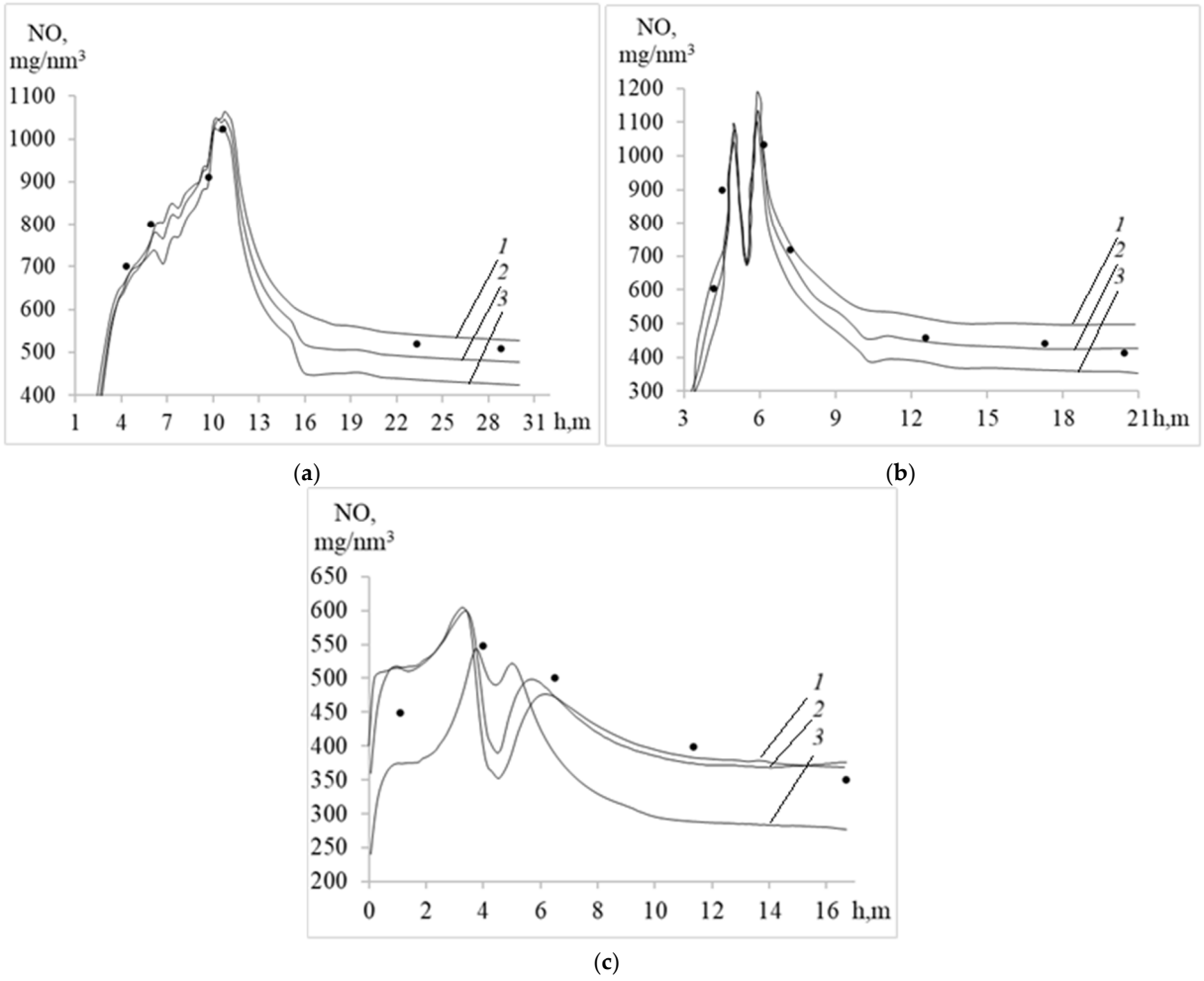

Figure 17. Distribution of nitrogen oxide concentration by the height of the combustion chambers of the studied boilers. (**a**) PK-39: curve 1—OFA = 0%; curve 2—OFA = 10%; curve 3—OFA = 20%; ● —experiment at a thermal power plant [40]. (**b**) BKZ-160: curve 1—OFA = 0%; curve 2—OFA = 10%; curve 3—OFA = 20%; ● —experiment at a thermal power plant [41]. (**c**) BKZ 75: curve 1—OFA = 0%; curve 2—OFA = 5%; curve 3—OFA = 18%; ● —experiment at a thermal power plant [41].

For the RK-39 boiler (Figure 17a), with a furnace chamber height of approximately 31 m, a pronounced peak in NO concentration is observed in the active combustion zone (7–13 m), reaching 1050 mg/Nm^3 at OFA = 0%. As the OFA share increases to 10% and 20%, the peak values decrease, and the outlet concentration is reduced from 527 to 423 mg/Nm^3. The experimental data reported in [40] are in good agreement with the calculated curves.

For the BKZ-160 boiler (Figure 17b), with a furnace chamber height of approximately 21 m, the NO profile is characterized by a sharper peak in the combustion zone (4–6 m), reaching 1150 mg/Nm^3 at OFA = 0%. The application of OFA (10% and 20%) leads to a significant reduction in the outlet NO concentration—from 498 to 352 mg/Nm^3—confirming the high effectiveness of this method. A reasonably good agreement is observed with the full-scale experimental data reported in [41].

For the BKZ-75 boiler (Figure 17c), with a furnace chamber height of approximately 16 m, a lower overall NO level is observed, along with a bimodal profile featuring concentration peaks at elevations of 2–3 m and 4–5 m. Increasing the OFA share from 0% to 18% reduces the outlet NO concentration from 368 to 277 mg/Nm^3 (25%) [41].

For all three boilers, a consistent trend is observed: increasing the proportion of overfire air (OFA) leads to a monotonic decrease in NO concentration at the furnace outlet. Furthermore, the calculated results are in good agreement with the experimental data reported in [40,41].

Table 3 presents the average temperature (T, °C) and NO concentration (mg/Nm^3) at the outlet of the furnace chambers of the RK-39, BKZ-160, and BKZ-75 boilers under different overfire air (OFA) supply conditions.

For the RK-39 boiler, increasing the OFA share from 0% to 20% is accompanied by a decrease in temperature from 1238.92 °C to 1200 °C and a reduction in NO concentration from 527.78 to 423.29 mg/Nm^3 (20%).

For the BKZ-160 boiler, a similar increase in OFA results in a decrease in NO concentration from 498.38 to 351.69 mg/Nm^3 (29%), while the temperature changes only slightly.

For the BKZ-75 boiler, increasing the OFA share from 0% to 18% reduces the NO concentration from 368.08 to 277.12 mg/Nm^3 (25%), accompanied by a decrease in temperature from 885.80 °C to 856.27 °C.

The greatest reduction in NO emissions was achieved for the BKZ-160 boiler (29.4%, from 498 to 352 mg/Nm^3). This is attributed to the compact furnace geometry (21 m in height), where the OFA jets provide intensive cross-flow mixing and create an extended fuel-rich reducing zone with an oxygen deficit. These conditions suppress both the thermal NO formation mechanism described by the Zeldovich mechanism (although the reduction in peak temperature from 1114 °C to 1107 °C is relatively small) and the fuel NO pathway through the reduction of NO by CH_i radicals.

For the RK-39 boiler, the reduction amounted to 19.8% (from 528 to 423 mg/Nm^3). The greater furnace height (30 m) decreases the effectiveness of OFA jet penetration and cross-sectional mixing; however, the substantial temperature reduction (from 1239 °C to 1200 °C) effectively suppresses the thermal Zeldovich mechanism, which is the dominant factor in NO reduction for this boiler.

For the BKZ-75 boiler, a 24.7% reduction (from 368 to 277 mg/Nm^3) is achieved primarily through the redistribution of oxygen within the combustion zones. The initially low temperature level (886 °C) indicates a relatively minor contribution of thermal NO formation; therefore, the main effect is associated with the fuel NO and prompt NO mechanisms. The bimodal NO concentration profile observed along the furnace height of the BKZ-75 boiler indicates the presence of spatially separated heat-release zones associated with alternating reducing and oxidizing regions—a phenomenon characteristic of a single-row burner arrangement.

Thus, the high sensitivity of NO concentration fields to the introduction of OFA, despite relatively small changes in the temperature profile, can be explained by the fact that the thermal mechanism is only one of three interacting NO_x reduction mechanisms. Moreover, its contribution varies significantly depending on the temperature regime of a particular boiler. Consequently, the overall effectiveness of OFA is determined not

only by temperature reduction but also by changes in oxygen distribution, combustion stoichiometry, and the enhancement of reducing reactions that suppress fuel and prompt NO formation pathways.

The obtained results confirm that the technology of staged combustion with additional air supply is an effective way to reduce NO_x emissions for boilers of different capacities and designs.

4. Conclusions

In the present study, CFD modeling based on the FLOREAN software package was employed for the numerical analysis of staged combustion (Overfire Air, OFA) processes in the furnace chambers of operating industrial boilers RK-39, BKZ-160, and BKZ-75 firing high-ash Kazakhstan coal (>40% ash content). The simulations were performed in a three-dimensional steady-state formulation using turbulence, combustion, and NO_x formation models adapted to the conditions of high-ash fuel combustion.

Satisfactory agreement was obtained between the simulation results and full-scale test data from operating thermal power plants, confirming the adequacy of the adapted FLOREAN software package for analyzing NO_x emissions in real power units.

A stable pattern was established for the distribution of NO along the furnace height, characterized by the formation of a maximum in the active combustion zone followed by a decrease in concentration in the upper part of the chamber. The identified profile indicates the dominance of the thermal mechanism of NO_x formation, controlled by local temperature and oxygen fields.

It was shown that the application of staged combustion technology with overfire air (OFA) supply provides a systematic reduction in NO concentration for all boilers studied, without loss of combustion stability. The effectiveness of the method depends significantly on the structural and aerodynamic features of the furnace chamber: the NO reduction amounted to 20% for the RK-39 boiler, 29% for the BKZ-160, and 25% for the BKZ-75, within an OFA fraction range of 5 to 18%. The lowest absolute NO_x emissions were recorded for the BKZ-75 boiler, attributable to the lower temperature level of the process, which limits the thermal mechanism.

For the first time, based on a comparative analysis of three boiler size types, it was shown that OFA effectiveness is determined not only by operating parameters but also by the geometry of the furnace chamber and the aerodynamic organization of the flame. In particular, the detected double-humped structure of the NO distribution indicates spatially separated heat release zones associated with the alternation of reducing and oxidizing regions. From an energy standpoint, the introduction of OFA leads to a moderate decrease in furnace outlet temperature, without negatively affecting the integral characteristics of the process.

The results obtained are consistent with published experimental and calculated data, confirming the technological feasibility of OFA as a primary method for reducing NO_x without significant reconstruction of boiler equipment. The adaptation of FLOREAN to high-ash coal conditions ensures reliable prediction of environmental protection measures and can be recommended for optimizing the operating modes of boilers of similar design.

Limitations of the study: the calculations were performed in a steady-state formulation, which does not account for unsteady combustion effects; verification was carried out for three boiler units of Kazakhstani type, and extending the results to boilers of a different design requires independent verification; the effect of OFA on carbon carryover and the intensity of slagging on heating surfaces requires a separate study.

Author Contributions: Conceptualization, A.A. and S.B. (Saltanat Bolegenova); methodology, A.A., V.M. and S.B. (Saltanat Bolegenova); validation, A.A., N.A. and S.B. (Saltanat Bolegenova); formal analysis, A.A., S.B. (Symbat Bolegenova) and S.O.; investigation, A.A., A.N. and S.B. (Symbat Bolegenova); writing—original draft preparation, A.A., S.B. (Symbat Bolegenova), V.M., S.B. (Saltanat Bolegenova), A.N. and N.A.; writing—review and editing, A.A., S.B. (Symbat Bolegenova), V.M., S.B. (Saltanat Bolegenova), A.N. and N.A.; software—V.M. and A.N.; supervision, A.A. All authors have read and agreed to the published version of the manuscript.

Funding: This work was supported by the Ministry of Education and Science of the Republic of Kazakhstan (No. AP26105185).

Data Availability Statement: The original contributions presented in this study are included in the article. Further inquiries can be directed to the corresponding author.

Conflicts of Interest: Author Nariman Askarov was employed by the company Kazatomprom National Atomic Company, Astana, Republic of Kazakhstan. The remaining authors declare that the research was conducted in the absence of any commercial or financial relationships that could be construed as potential conflicts of interest.

Abbreviations

TPP	Thermal power plant
CFD	Computational fluid dynamics
OFA	Overfire Air
BKZ	drum boiler unit;
PK	pulverized coal boiler.
EDM	Eddy Dissipation Model
CBTI	Central Boiler and Turbine Institute

References

1. Abdulbarova, Y. Ugol' v Mire: Dobycha, Eksport, Import, Zapasy, Primenenie, Perspektivy. Available online: https://lindeal.com/trends/ugol-v-mire-dobycha-ehksport-import-zapasy-primenenie-perspektivy?ysclid=mp80sly8a9799228901 (accessed on 1 January 2023).
2. MEA: Vysokij Spros na Ugol' Sohranitsya v 2026 Godu. Available online: https://itek.ru/news/mea-vysokij-spros-na-ugol-sohranitsya-v-2026-godu/?ysclid=mp80nl88d1197481545 (accessed on 24 July 2023).
3. Ibraeva, S. Ugol' Vozvrashchaetsya: Kak Vojna na Blizhnem Vostoke Menyaet Klimaticheskuyu Politiku Mira. Available online: https://ulysmedia.kz/pozitsiya/71270-ugol-vozvrashchaetsia-kak-voina-na-blizhnem-vostoke-meniaet-klimaticheskuiu-politiku-mira/ (accessed on 7 April 2026).
4. Novikova, A. Pochemu Kazakhstan Poka ne Mozhet Otkazat'sya ot Ugol'noj Generacii. Available online: https://otyrar.kz/2025/11/pochemu-kazahstan-poka-ne-mozhet-otkazatsya-ot-ugolnoj-generaczii/?ysclid=mp5ghliv9u614789540 (accessed on 8 November 2025).
5. Baidildenov, Z. Kazakhstan i Ugol'naya Generaciya: Vozmozhen li Otkaz, Chto Zhdet Eksport. Available online: https://freshnews.kz/kazahstan-i-ugolnaya-generacziya-vozmozhen-li-otkaz-chto-zhdet-eksport/ (accessed on 30 April 2025).
6. Wu, X.; Liu, N.; Lu, Y.; Chen, Z.; Li, Z. Numerical Simulation of the OFA Effect on Combustion in a 600 MWe Boiler with Centrally Fuel Rich Burners. *Combust. Sci. Technol.* **2025**, *197*, 5098–5116. [CrossRef]
7. Chen, J.; Yang, W.; He, Y.; Wang, Z.; Liu, J. The characteristics of NO reduction with multiple over-fire air (OFA)-staged combustion. *J. Energy Inst.* **2025**, *122*, 102216. [CrossRef]
8. Su, X.; Ma, L.; Yao, B.; Liao, W.; Zheng, Y.; Miao, M.; Fang, Q.; Chen, G.; Yang, W. High-efficiency combustion and low-nitrogen emission of coal-fired boiler based on synergistic optimization of swirl burner structure and air-staged technology. *Fuel* **2025**, *388*, 134352. [CrossRef]
9. Bolegenova, A.; Askarova, A.; Nugymanova, A.; Maximov, V.; Bolegenova, S.; Askarov, N.; Ospanova, S.; Shortanbayeva, Z. Implementing overfire air technology in coal-fired power plants to promote environmentally friendly energy generation. *Energies* **2026**, *19*, 347. [CrossRef]
10. Leithner, R.; Müller, H. CFD Studies for Boilers. In Proceedings of the Second M.I.T. Conference on Computational Fluid and Solid Mechanics, Cambridge, MA, USA, 17–20 June 2003. Available online: https://www.sciencedirect.com/book/edited-volume/9780080440460/computational-fluid-and-solid-mechanics-2003 (accessed on 1 June 2026).

11. Leithner, R.; Müller, H.; Fischer, K.; Schiller, A. Optimierung der Simulation von Feuerungen. In *Proceedings of the Deutscher Flammentag 1999*; VDI Berichte: Düsseldorf, Germany, 1999; Volume 1492, pp. 63–68. Available online: https://www.tib.eu/de/suchen/id/BLCP:CN031767261/Optimierung-der-Simulation-von-Feuerungen?cHash=10d50ecc0a0aa8d390b36093dd2cc1b0 (accessed on 1 June 2026).
12. Dobrowolski, R.; Löhr, T.; Leithner, R. Simulation und Optimierung von Kraftwerksprozessen. In *Proceedings of the Modellierung und Simulation von Dampferzeugern und Feuerungen*; VDI Berichte: Düsseldorf, Germany, 1998; Volume 1390, pp. 109–126. Available online: https://www.tib.eu/de/suchen/id/TIBKAT:271848596/Modellierung-und-Simulation-von-Dampferzeugern?cHash=0998efa9f62b3b5e9647f99250b8c9e3 (accessed on 1 June 2026).
13. Kang, W.; Jo, H.; Lee, J.; Jang, K.; Ryu, C. Numerical investigations on overfire air design for improved boiler operation and lower NOx emission in commercial wall-firing coal power plants. *Appl. Therm. Eng.* **2023**, *219*, 119604. [CrossRef]
14. Jin, W.; Si, F.; Kheirkhah, S.; Yu, C.; Li, H.; Wang, Y. Numerical study on the effects of primary air ratio on ultra-low-load combustion characteristics of a 1050 MW coal-fired boiler considering high-temperature corrosion. *Appl. Therm. Eng.* **2023**, *221*, 119811. [CrossRef]
15. Wang, H.; Jin, H.; Yang, Z.; Deng, S.; Wu, X.; An, J.; Sheng, R.; Ti, S. CFD modeling of flow, combustion and NOx emission in a wall-fired boiler at different low-load operating conditions. *Appl. Therm. Eng.* **2024**, *236*, 121824. [CrossRef]
16. Wang, Y.; Zhou, Y. Numerical optimization of the influence of multiple deep air-staged combustion on the NOx emission in an opposed firing utility boiler using lean coal. *Fuel* **2020**, *269*, 116996. [CrossRef]
17. Zha, Q.; Li, D.; Wang, C.; Che, D. Numerical evaluation of heat transfer and NOx emissions under deep-air-staging conditions within a 600 MWe tangentially fired pulverized-coal boiler. *Appl. Therm. Eng.* **2017**, *116*, 170–181. [CrossRef]
18. Han, J.; Han, L.; Lu, Y.; Mu, Y.; Mustafa, A.; Ge, Y. Numerical simulation of combustion in 35 t/h industrial pulverized coal furnace with burners arranged on front wall. *Processes* **2020**, *8*, 1272. [CrossRef]
19. Darbandi, M.; Fatin, A.; Bordbar, H. Numerical study on NOx reduction in a large-scale heavy fuel oil-fired boiler using suitable burner adjustments. *Energy* **2020**, *199*, 117371. [CrossRef]
20. Adamczyk, W.P.; Isaac, B.; Parra-Alvarez, J.; Smith, S.T.; Harris, D.; Thornock, J.N.; Zhou, M.; Smith, P.J.; Żmuda, R. Application of LES-CFD for predicting pulverized-coal working conditions after installation of NOx control system. *Energy* **2018**, *160*, 693–709. [CrossRef]
21. Müller, H. *Numerische Berechnung Dreidimensionaler Turbulenter Strömungen in Dampferzeugern mit Wärmeübergang und Chemischen Reaktionen*; VDI-Verlag: Düsseldorf, Germany, 1992. Available online: https://bonnus.ulb.uni-bonn.de/discovery/fulldisplay?vid=49HBZ_ULB:DEFAULT&docid=alma991015544579706467&context=L (accessed on 1 June 2026).
22. Epple, B.; Leithner, R.; Linzer, W.; Walter, H. (Eds.) *Simulation von Kraftwerken und Wärmetechnischen Anlagen*; Springer: Vienna, Austria, 2009; ISBN 978-3-211-29695-0. [CrossRef]
23. Askarova, A.S.; Bolegenova, S.A.; Georgiev, A.; Bolegenova, S.A.; Maximov, V.Y.; Manatbayev, R.K.; Yergaliyeva, A.B.; Nugymanova, A.O.; Baizhuma, Z.T. The use of a new "clean" technology for burning low-grade coal in boilers of Kazakhstan TPPs. *Bulg. Chem. Commun.* **2018**, *50*, 53–60.
24. Zhu, B.; Shang, B.; Guo, X.; Chen, X.; Zhao, L. Study on combustion characteristics and NO_x formation in 600 MW coal-fired boiler based on numerical simulation. *Energies* **2023**, *16*, 262. [CrossRef]
25. Askarova, A.S.; Bolegenova, S.A.; Bolegenova, S.A.; Maximov, V.Y.; Beketayeva, M.T. Modeling of heat mass transfer in high-temperature reacting flows with combustion. *High Temp.* **2018**, *56*, 738–743. [CrossRef]
26. Modliński, N.; Szczepanek, K. Numerical studies of the influence of flue gas recirculation into primary air on NOx formation, co emission, and low-NO_x waterwall corrosion in the OP 650 boiler. *Energies* **2024**, *17*, 2227. [CrossRef]
27. Wang, W.; Yang, M. Numerical and experimental study on nonlinear phenomena and thermal deviation control in a 1000 mw tower-type boiler. *Energies* **2024**, *17*, 1329. [CrossRef]
28. Messerle, V.E.; Askarova, A.S.; Ustimenko, A.B.; Karpenko, E.I.; Loktionova, I.V. Optimization of the combustion of power station coals using plasma technologies. *Therm. Eng.* **2004**, *51*, 488–493.
29. Modliński, N.; Madejski, P.; Janda, T.; Szczepanek, K.; Kordylewski, W. A Validation of computational fluid dynamics temperature distribution prediction in a pulverized coal boiler with acoustic temperature measurement. *Energy* **2015**, *92*, 77–86. [CrossRef]
30. Jiang, L.; Zhou, T.; Suo, S.; Dai, Y.; Hamid, M.O.A.; Zhang, Y.; Qi, H.; Yang, X.; Xie, M. Visualization on the turbulent structure and restructure characteristic in the wake of a packed bed reactor: PIV measurements and POD analysis. *Renew. Energy* **2025**, *246*, 122895. [CrossRef]
31. Xie, W.; Luo, Z.; Wang, H.; Zhou, Y.; Liu, Q.; Zhu, Y. Experimental investigation on double wedge type-V shock/shock interaction control subject to SparkJet array. *Acta Mech. Sin.* **2026**, *42*, 125207. [CrossRef]
32. Launder, B.; Spalding, D. The numerical computation of turbulent flows. *Comp. Meths. Appl. Mech. Eng.* **1974**, *3*, 269–289. [CrossRef]

33. Versteeg, H.K.; Malalasekera, W. *An Introduction to Computational Fluid Dynamics: The Finite Volume Method*, 2nd ed.; Pearson Education: Harlow, UK, 2007; ISBN 978-0-13-127498-3. Available online: https://books.google.kz/books?id=RvBZ-UMpGzIC&redir_esc=y (accessed on 1 June 2026).
34. Lockwood, F.; Shah, N. An improved flux model for calculation of radiation heat transfer in combustion chambers. In Proceedings of the 16th National Heat Transfer Conference, St. Louis, MO, USA, 9–11 August 1976; pp. 2–7. Available online: https://ui.adsabs.harvard.edu/abs/1976ceht.conf.....L/abstract (accessed on 1 June 2026).
35. Harmor, R.J. Kinetics of combustion of pulverized brown coal char. *Combust. Flame* **1973**, *21*, 153–162. [CrossRef]
36. Magnussen, B.F.; Hjertager, B.H. On mathematical modeling of turbulent combustion with special emphasis on soot formation and combustion. *Symp. (Int.) Combust.* **1977**, *16*, 719–729. [CrossRef]
37. Belosevic, S.V.; Tomanovic, I.D.; Crnomarkovic, N.D.; Milićević, A.R.; Tucaković, D.R. Modeling and optimization of processes for clean and efficient pulverized coal combustion in utility boilers. *Therm. Sci.* **2016**, *20*, 183–196. [CrossRef]
38. De Soete, G.G. Overall reaction rates of NO and N_2 formation from fuel nitrogen. *Symp. (Int.) Combust.* **1975**, *15*, 1093–1102. [CrossRef]
39. Mitchell, J.W.; Tarbell, J.M. A kinetic model of nitric oxide formation during pulverized coal combustion. *AIChE J.* **1982**, *28*, 302–311. [CrossRef]
40. Akimbek, G.; Aliyarov, B.; Sakhmetova, G.; Kalambaeva, G. Investigation of the effect of burner diameter to outflow velocity ratio on combustion parameters in steam boiler PK-39. *Vestn. KazATK* **2025**, *137*, 483–491. [CrossRef]
41. Aliyarov, A.B.; Aliyarov, B.K.; Aliyarova, M.B. *Heat Energy Supply in Kazakhstan*; Textbook; Gylym Ordasy: Almaty, Kazakhstan, 2012. Available online: https://www.almanah.kz/books/energetika/snabzhenie-teplovoy-energiey-v-kazakhstane-uchebnik/ (accessed on 1 January 2021).
42. *Thermal Calculation of Boilers (Normative Method)*, 3rd ed.; NPO CKTI: Saint Petersburg, Russia, 1998; 256p. Available online: https://portal.tpu.ru/SHARED/j/JANKOVSKY/education/%D0%9D%D0%BE%D1%80%D0%BC%D1%8B.pdf (accessed on 1 June 2026).

Disclaimer/Publisher's Note: The statements, opinions and data contained in all publications are solely those of the individual author(s) and contributor(s) and not of MDPI and/or the editor(s). MDPI and/or the editor(s) disclaim responsibility for any injury to people or property resulting from any ideas, methods, instructions or products referred to in the content.